P and Si functionalized MXenes for metal-ion battery applications

2D Materials

PAPER

RECEIVED
22 December 2016

REVISED
19 March 2017

ACCEPTED FOR PUBLICATION
29 March 2017

PUBLISHED
10 April 2017

P and Si functionalized MXenes for metal-ion battery applications

Jiajie Zhu[1,2] and Udo Schwingenschlögl[2]

[1] College of Materials Science and Engineering, Shenzhen University, Nanhai Ave 3688, ShenZhen, Guangdong 518060, People's Republic of China

[2] King Abdullah University of Science and Technology (KAUST), Physical Science and Engineering Division (PSE), Thuwal 23955-6900, Saudi Arabia

E-mail: udo.schwingenschlogl@kaust.edu.sa

Keywords: MXene, 2D material, battery

Abstract

MXenes are a family of two-dimensional materials, composed of early transition metal carbides, nitrides, and carbonitrides, with great potential in energy storage systems, in particular in electrodes for Li, Na, K-ion batteries. However, so far the capacities are not competitive. In this context, we investigate P and Si functionalized MXenes for metal-ion battery applications, using first-principles calculations, since P and Si provide reaction products with high ion content. Replacement of the F and OH ligands of Ti_2C and V_2C with P and Si is demonstrated to be feasible (energy barriers of less than 0.128 eV) and the ion diffusion barriers turn out to be less than 0.32 eV. Importantly, the Li, Na, and K capacities are predicted to be 1767 mAh g^{-1}, 711 mAh g^{-1}, and 711 mAh g^{-1}, respectively, thus being much higher than in the case of F and OH functionalization.

1. Introduction

Li-ion batteries nowadays are widely used in portable electronic devices such as cell phones and laptops due to high energy densities, absence of memory effects, and long cycle lifes [1]. Na and K-ion batteries have been considered as promising alternatives in large scale applications such as power grids, since Na and K have similar properties to Li combined with the advantage of natural abundance [2, 3]. The Li, Na, and K capacities of graphite (commercial electrode material), however, are only 372 mAh g^{-1} [1], 284 mAh g^{-1} [4], and 273 mAh g^{-1} [5], respectively. Bulk P and Si electrodes have theoretical Na and Li capacities of 2596 mAh g^{-1} [6] and 4198 mAh g^{-1} [7], respectively, due to the formation of Na_3P and $Li_{22}Si_5$. Regrettably, the huge volume changes of 420% and 491%, respectively, lead to rapid capacity loss and safety issues during charging and discharging. Dimension reduction from bulk to two or one-dimensional electrode materials has been able to partially overcome these issues, since the void space in the low-dimensional structures can accommodate strain and volume changes [8–10].

MXenes are two-dimensional early transition metal carbides, nitrides, and carbonitrides, such as Ti_2C, V_2C, Ti_3C_2, Ti_3CN, and Ta_4C_3 [11, 12]. They can be synthesized by selective etching of the A element from MAX phases (M: early transition metal, A: group 13–16 element, X: C and/or N) [13]. MXenes are considered to have great application potential in electronic devices [14, 15], catalysis [16], and energy storage [17]. Like other two-dimensional materials [18, 19], they also have been proposed for Li-ion batteries due to Li capacities comparable to commercial graphite electrodes and stable cycling performance [20]. Furthermore, the application in Na and K-ion batteries has been explored [21]. The Li capacity of MXenes currently is limited by 410 mAh g^{-1} [20], which is much lower than that of P [6] and Si [7]. While the Li capacity of V_2C has been predicted to be 940 mAh g^{-1} (based on a multilayer model) [22], the experimental value is only 260 mAh g^{-1} [23]. The Na and K capacities are usually lower than the Li capacity due to larger ionic radii [24].

MXenes are usually functionalized by F and OH ligands as a consequence of the presence of HF and H_2O during the preparation [25]. These ligands come along with lower Li content in the products (LiF and LiOH) than P and Si (Li_3P and $Li_{22}Si_5$) and thus lead to lower Li capacities. Therefore, we investigate in the present work the feasibility of replacing the F and OH ligands with P and Si, using first-principles calculations. Aiming for metal-ion battery applications, it is promising to improve the capacities by this approach, since the crystal structure of MXenes can accommodate large volume changes. The Sc_2C, Ti_2C, and V_2C MXenes are selected due to their small atomic masses and the fact that they provide different numbers of valence electrons.

Table 1. Formation energies of the F, OH, P, and Si ligands and enthalpies of the F → LiF and OH → LiOH conversion reactions (eV per ligand).

	F	F → LiF	OH	OH → LiOH	P	Si
Sc_2C	−6.208	0.085	−5.943	0.551	—	—
Ti_2C	−5.523	−0.600	−5.520	0.128	−1.331	−0.498
V_2C	−4.746	−1.376	−4.847	−0.545	−1.514	−0.825

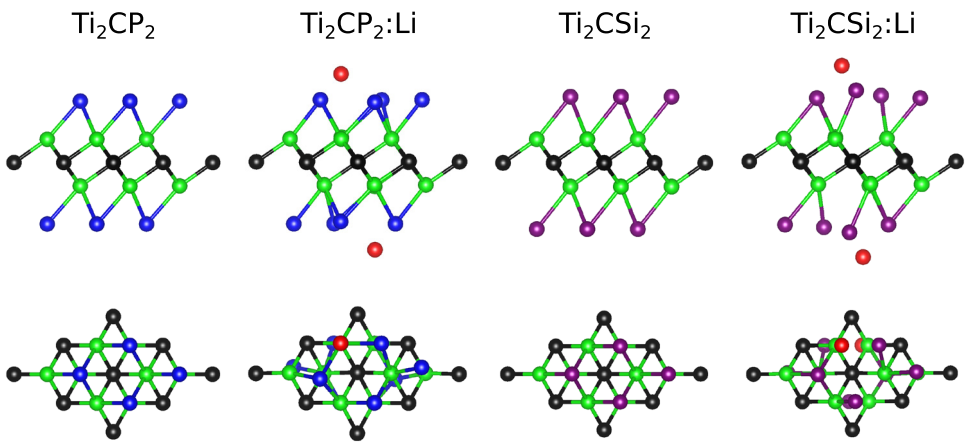

Figure 1. Side (upper row) and top (lower row) views of the structures of Ti_2CP_2 and Ti_2CSi_2 without and with Li decoration. The Ti, C, P, Si, and Li atoms are shown in green, black, blue, purple, and red color.

2. Computational method

We perform adsorption calculations based on density functional theory and the projector augmented wave method, as implemented in the Vienna *ab initio* simulation package [26]. The generalized gradient approximation of Perdew, Burke and Ernzerhof is selected for the exchange-correlation potential together with the DFT-D3 approach [27] to take into account the long-range van der Waals interaction. A vacuum layer of 15 Å thickness is added on top of 2×2 in-plane supercells of the MXenes in order to avoid artificial interaction between periodic images. For the Brillouin zone integrations we use a $6 \times 6 \times 1$k-mesh. The cutoff energy of the plane wave basis is set to 500 eV and the energy criterion of the iterative solution of the Kohn–Sham equations to 10^{-6} eV. All structures are relaxed until the residual forces on the atoms have declined to less than 0.01 eV $Å^{-1}$. We find spin degeneracy in each case. The diffusion paths and energy barriers are determined by the nudged elastic band method [28] with 9 images between the initial and final states.

3. Results and discussion

The formation energies of the F and OH ligands, defined as (M = Sc, Ti, V and X = F, OH, P, Si)

$$\Delta H = E[M_2CX_2] - E[M_2C] - 2E[X], \qquad (1)$$

with E being the total energy, are calculated to be more negative than −4 eV, see table 1, and therefore reflect chemical stability. $E[X]$ is half of the total energy of F_2 for F, half of the sum of the total energies of O_2 and H_2 for OH, and the total energy per atom of the respective bulk compound for P and Si. The conversion reaction

$$M_2CF_2 + 2Li \rightarrow M_2C + 2LiF \qquad (2)$$

for F turns out to be neutral for Sc_2C and exothermic for Ti_2C and V_2C. It thus is feasible to remove the ligand from the MXenes. The conversion reaction

$$M_2C(OH)_2 + 2Li \rightarrow M_2C + 2LiOH \qquad (3)$$

for OH is endothermic and exothermic for Sc_2C and V_2C, respectively. The reaction enthalpy for Ti_2C turns out to be 0.128 eV, which is slightly endothermic but less than for Zr_2CO_2/Zr_2CS_2 interconversion (0.611 eV at 298 K) [29]. Although the reaction enthalpies are calculated at 0 K, these findings are qualitatively valid also at high temperature, because the entropy and temperature corrections are estimated to be only 0.026 eV at room temperature when gas phases are involved [25]. The low reaction enthalpy can be overcome by sonication, which is a standard method in the preparation of MXenes.

Table 2. Structural parameters: M-X bond length (b, in Å), vertical distance between the M and X atoms (d, in Å), and charge transfer from X to M_2C (Δq, in electrons).

	Ti_2CP_2	V_2CP_2	Ti_2CSi_2	V_2CSi_2
b	2.62	2.46	2.74	2.67
d	1.97	1.81	2.15	2.12
Δq	−0.50	−0.38	−0.41	−0.27

Turning to the feasibility of P and Si functionalization of Ti_2C and V_2C, we consider locations on top of the C atom and on top of the lower and upper Ti/V atoms. Figure 1 shows the lowest energy structures resulting

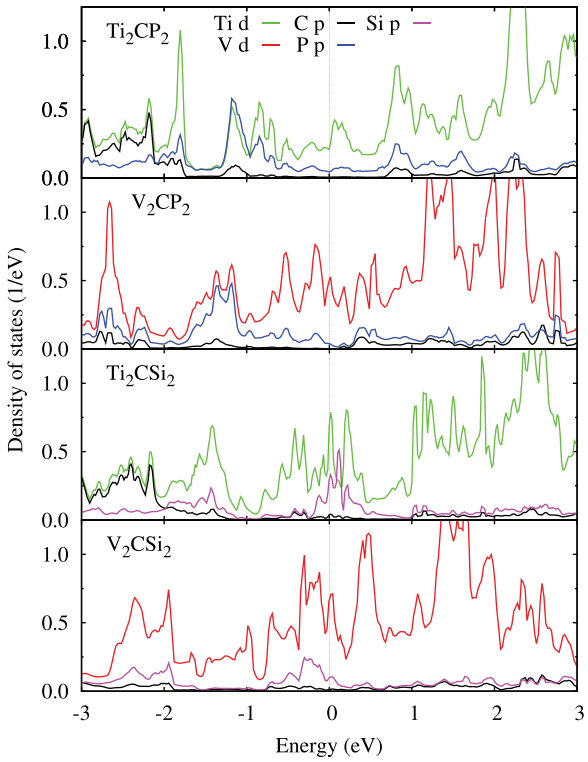

Figure 2. Orbitally resolved densities of states of Ti_2CP_2, V_2CP_2, Ti_2CSi_2, and V_2CSi_2.

Table 3. Structural parameters: vertical distance between the X and Li/Na/K atoms (ℓ, in Å) and charge transfer from Li/Na/K to M_2CX_2 (Δm, in electrons).

		Ti_2CP_2	V_2CP_2	Ti_2CSi_2	V_2CSi_2
Li	ℓ	1.29	1.39	1.52	1.68
Li	Δm	0.86	0.84	0.84	0.84
Na	ℓ	1.69	1.95	1.96	2.12
Na	Δm	0.79	0.77	0.76	0.75
K	ℓ	2.18	2.41	2.40	2.53
K	Δm	0.76	0.71	0.75	0.73

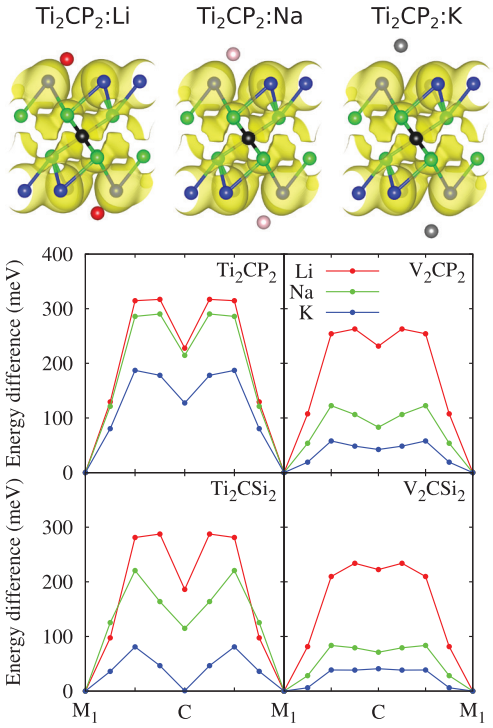

Figure 3. Top: charge density for Li/Na/K-decorated Ti_2CP_2 (isosurface value: 0.03 electrons/bohr^3). The Ti, C, P, Li, Na, and K atoms are shown in green, black, blue, red, pink, and grey color. Bottom: energy barriers for Li/Na/K diffusion on Ti_2CP_2, V_2CP_2, Ti_2CSi_2, and V_2CSi_2.

from our relaxations. Negative formation energies, see table 1, reflect stability in each case. We find that P obtains more charge (calculated by the Bader approach) from the MXenes than Si due to its larger electronegativity, see table 2. In addition, V_2C transfers less charge to the ligands than Ti_2C, which agrees with a more covalent bonding character with shorter bond lengths. The functionalized MXenes are metallic, see the densities of states in figure 2, as required for battery applications. The Ti/V 3*d* states dominate around the Fermi level. In the case of Si functionalization there is also a significant amount of Si 3*p* states, much more than P 3*p* states in the case of P functionalization, reflecting reduced stability.

Three locations are considered for Li/Na/K, namely on top of the M atom in the first layer (M_1), the C atom, and the M atom in the second layer (M_2). The M_1 site turns out to be energetically favorable and therefore is shown in figure 1. We obtain for Ti_2CP_2 and V_2CP_2 almost identical formation energies of −1.0 eV, −0.7 eV, and −0.6 eV for Li, Na, and K, respectively. On the other hand, the formation energies for V_2CSi_2 (−2.0 eV, −1.7 eV, and −2.0 eV) and Ti_2CSi_2 (−1.5 eV, −1.3 eV, and −1.5 eV) are not the same due to differ-

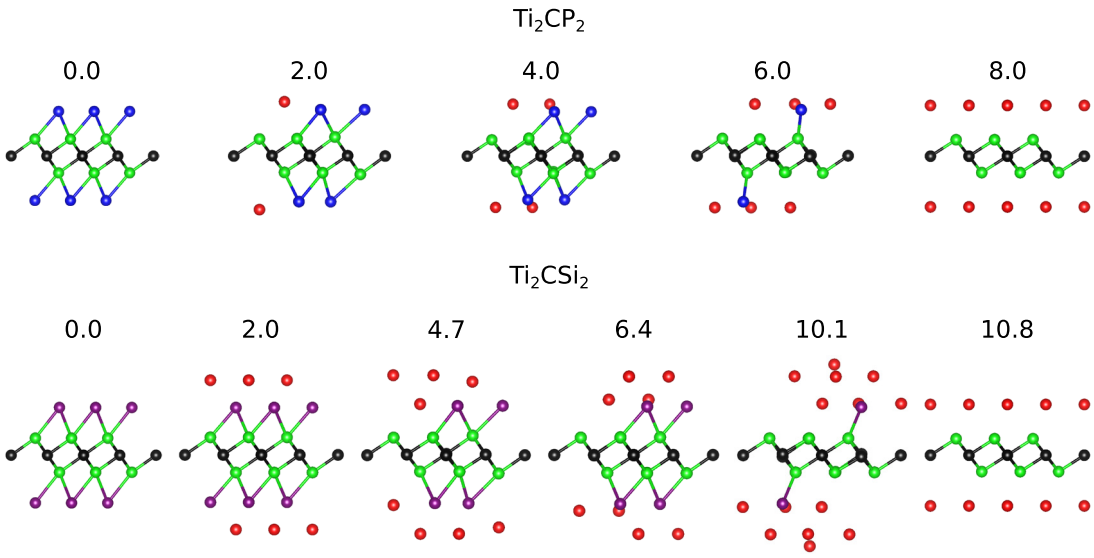

Figure 4. Side views of Ti_2CP_2 and Ti_2CSi_2 for different Li coverages. The Ti, C, P, Si, and Li atoms are shown in green, black, blue, purple, and red color.

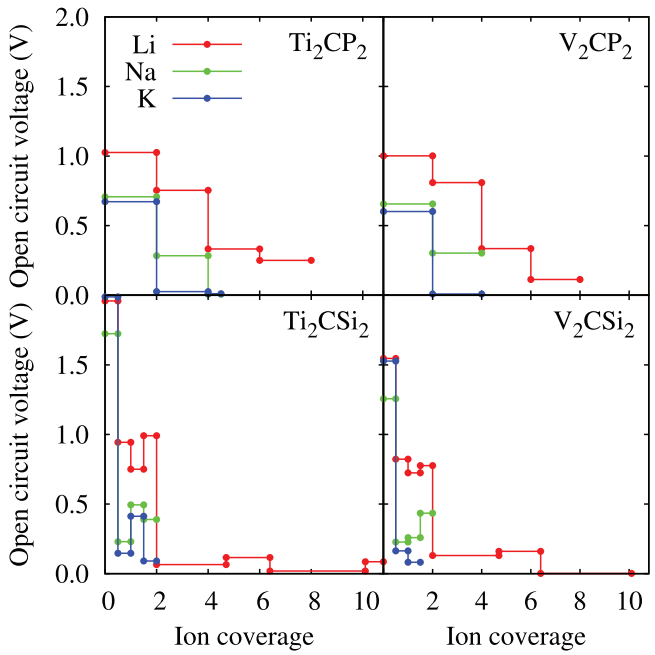

Figure 5. Open circuit voltages as functions of the Li/Na/K coverage.

ences in the relaxation of the ligands. The vertical distance between the X and Li/Na/K atoms increases from Li to K, see table 3, because of the growing ionic radius. This effect lowers the charge transfer.

The energy barriers for Li/Na/K diffusion on Ti_2CP_2, V_2CP_2, Ti_2CSi_2, and V_2CSi_2 are addressed in figure 3. The path connecting two M_1 sites through the C site provides lower energy barriers than that through the M_2 site as well as the direct connection. The diffusion barriers decrease from Li to K, since an adatom farther away from the ligand is less influenced by charge density fluctuations. The transition states are located near the middle between the M_1 and C sites, leaning towards the C site. The obtained Li diffusion barriers (0.32 eV, 0.26 eV, 0.29 eV, and 0.23 eV for Ti_2CP_2, V_2CP_2, Ti_2CSi_2, and V_2CSi_2, respectively)

Table 4. Comparison of the Li/Na/K capacities (in mAh g^{-1}) obtained for the materials under consideration.

	Ti_2CP_2	V_2CP_2	Ti_2CSi_2	V_2CSi_2
Li	1264	1220	1767	1592
Na	711	610	327	315
K	711	610	327	236

are comparable to those of F functionalized MXenes ($Ti_3C_2F_2$: 0.36 eV [30], Ti_2CF_2: 0.30 eV, V_2CF_2: 0.28 eV) and other two-dimensional materials (silicene: 0.23 eV [31], MoS_2: 0.21 eV [32]).

Structures of Ti_2CP_2 decorated with different amounts of Li atoms are illustrated in figure 4. By reaction with three Li atoms, each P atom is converted in the lithiation process (forming Li_3P). Simultaneously, the created vacancy is filled by another Li atom, reflecting alternation of conversion and intercalation reactions. Results for the open circuit voltage

$$V = -(E(x_2) - E(x_1))/(x_2 - x_1) - E[\text{Li/Na/K}], \quad (4)$$

where $E(x)$ is the total energy of the full system with Li/Na/K coverage x [33], are shown in figure 5. The value decreases for Ti_2CP_2 (V_2CP_2) from 1.0 V to 0.2 V (0.1 V) when the Li coverage increases to 8 atoms per formula unit. Overall the lithiation process is similar for Ti_2CP_2 and V_2CP_2, whereas the open circuit voltage at high Li coverage is lower for V_2CP_2 (because the formation energy of P is more negative). We calculate the (specific) capacity as

$$C = x \cdot F/M, \quad (5)$$

where F and M, respectively, are the Faraday constant and atomic mass of the material without adsorbed atoms [33]. Values of 1264 mAh g^{-1} and 1220 mAh g^{-1} (table 4) are found for Ti_2CP_2 and V_2CP_2, respectively, being much higher than corresponding values for F and OH functionalized MXenes (410 mAh g^{-1}) [20] as well as for graphite (372 mAh g^{-1}) [33]. The sodiation and potassiation processes of Ti_2CP_2 and V_2CP_2 turn out to be similar to the lithiation process but yield lower voltages due to weaker interaction between the ions and ligands. Low cohesive energies of the products lead to lower (and identical) Na and K capacities as compared to the Li capacity of both Ti_2CP_2 (711 mAh g^{-1}) and V_2CP_2 (610 mAh g^{-1}). Although P can be converted only partially in the sodiation and potassiation processes due to this reason, the values are still higher than reported for bare MXenes [24] and graphite [33].

Si cannot be converted until Ti_2CSi_2 is fully intercalated by 2 Li atoms per formula unit, see figure 4. While the conversion process itself is similar to the case of Ti_2CP_2, the number of intercalated Li atoms varies. The maximal Li coverage turns out to be 10.8, exceeding that of Ti_2CSi_2 as the Li content is higher in $Li_{22}Si_5$ than Li_3P. Consequently, a higher Li capacity of 1767 mAh g^{-1} is obtained. The corresponding Li capacity of V_2CSi_2 is only 1592 mAh g^{-1} as the last Si atom shows higher stability and thus cannot be converted. Ti_2CSi_2 and V_2CSi_2 can only be intercalated by 1 Na or K atom per formula unit, so that the Na and K capacities are much lower.

4. Conclusions

Replacement of the standard F and OH ligands of MXenes with P and Si has been studied by first-principles calculations, aiming at improvement of the material properties for metal-ion battery applications. Removal of the F and OH ligands from Ti_2C and V_2C by reaction with Li is predicted to be feasible. In addition, both P and Si are found to be stable ligands on the two MXenes and to preserve metallicity. The diffusion barrier decreases from Li (0.32 eV) to Na (0.29 eV) and to K (0.19 eV), as in F functionalized MXenes. P and Si are fully converted during the lithiation process, delivering Li capacities (1264 mAh g^{-1} and 1767 mAh g^{-1}, respectively) much higher than reported earlier for F and OH functionalized MXenes. Although the ligands can only be converted partially in the sodiation and potassiation processes, the corresponding capacities of 711 mAh g^{-1} still clearly exceed those of bare MXenes and graphite. F and OH ligands can be removed from MXenes by sonication assisted reaction with Li, resulting in high chemical activity for P and Si functionalization. The enhancement of the Li/Na/K capacity by P and Si functionalization will significantly improve the performance of MXenes in metal-ion battery applications.

Acknowledgments

The research reported in this publication was supported by funding from King Abdullah University of Science and Technology (KAUST).

References

[1] Jing Y, Zhou Z, Cabrera C R and Chen Z 2014 Graphene, inorganic graphene analogs and their composites for lithium ion batteries *J. Mater. Chem.* A **2** 12104–22
[2] Kubota K and Komaba S 2015 Review–practical issues and future perspective for Na-ion batteries *J. Electrochem. Soc.* **162** A2538–50
[3] Luo W *et al* 2015 Potassium ion batteries with graphitic materials *Nano Lett.* **15** 7671–7
[4] Wen Y, He K, Zhu Y, Han F, Xu Y, Matsuda I, Ishii Y, Cumings J and Wang C 2014 Expanded graphite as superior anode for sodium-ion batteries *Nat. Commun.* **5** 4033
[5] Jian Z, Luo W and Ji X 2015 Carbon electrodes for K-ion batteries *J. Am. Chem. Soc.* **137** 11566–9
[6] Qian J, Wu X, Cao Y, Ai X and Yang H 2013 High capacity and rate capability of amorphous phosphorus for sodium ion batteries *Angew. Chem., Int. Ed.* **52** 4633–6
[7] Wu X L, Guo Y G and Wan L J 2013 Rational design of anode materials based on group iva elements (Si, Ge, and Sn) for lithium-ion batteries *Chem. Asian J.* **8** 1948–58
[8] Xu K, Ben L, Li H and Huang X 2015 Silicon-based nanosheets synthesized by a topochemical reaction for use as anodes for lithium ion batteries *Nano Res.* **8** 2654–62
[9] Wan J *et al* 2014 Two dimensional silicon nanowalls for lithium ion batteries *J. Mater. Chem.* A **2** 6051–7
[10] He M, Kravchyk K, Walter M and Kovalenko M V 2014 Monodisperse antimony nanocrystals for high-rate Li-ion and Na-ion battery anodes: nano versus bulk *Nano Lett.* **14** 1255–62
[11] Naguib M, Mochalin V N, Barsoum M W and Gogotsi Y 2014 25th anniversary article: MXenes: a new family of two-dimensional materials *Adv. Mater.* **26** 992–1005
[12] Lei J C, Zhang X and Zhou Z 2015 Recent advances in MXene: preparation, properties, and applications *Front. Phys.* **10** 276–86
[13] Barsoum M W 2013 *MAX Phases: Properties of Machinable Ternary Carbides and Nitrides* (Weinheim: Wiley)
[14] Lee Y, Hwang Y, Cho S B and Chung Y C 2014 Achieving a direct band gap in oxygen functionalized-monolayer scandium carbide by applying an electric field *Phys. Chem. Chem. Phys.* **16** 26273–8

[15] Ma Z, Hu Z, Zhao X, Tang Q, Wu D, Zhou Z and Zhang L 2014 Tunable band structures of heterostructured bilayers with transition-metal dichalcogenide and MXene monolayer *J. Phys. Chem.* C **118** 5593–9
[16] Wang F, Yang C, Duan C, Xiao D, Tang Y and Zhu J 2015 An organ-like titanium carbide material (MXene) with multilayer structure encapsulating hemoglobin for a mediator-free biosensor *J. Electrochem. Soc.* **162** B16–21
[17] Hu Q, Sun D, Wu Q, Wang H, Wang L, Liu B, Zhou A and He J 2013 Mxene: a new family of promising hydrogen storage medium *J. Phys. Chem.* A **117** 14253–60
[18] Zhao X, Zhang X, Wu D, Zhang H, Ding F and Zhou Z 2016 *Ab initio* investigations on bulk and monolayer V_2O_5 as cathode materials for Li-, Na-, K- and Mg-ion batteries *J. Mater. Chem.* A **4** 16606–11
[19] Tang Q, Zhou Z and Chen Z2015 Innovation and discovery of graphene-like materials via density-functional theory computations *WIREs Comput. Mol. Sci.* **5** 360–79
[20] Mashtalir O, Naguib M, Mochalin V N, Dall'Agnese Y, Heon M, Barsoum M W and Gogotsi Y 2013 Intercalation and delamination of layered carbides and carbonitrides *Nat. Commun.* **4** 1716
[21] Xie Y, DallAgnese Y, Naguib M, Gogotsi Y, Barsoum M W, Zhuang H L and Kent P R C 2014 Prediction and characterization of MXene nanosheet anodes for non-lithium-ion batteries *ACS Nano* **8** 9606–15
[22] Hu J, Xu B, Ouyang C, Yang S A and Yao Y 2014 Investigations on V_2C and V_2CX_2 (X = F, OH) monolayer as a promising anode material for Li ion batteries from first-principles calculations *J. Phys. Chem.* C **118** 24274–81
[23] Naguib M, Halim J, Lu J, Cook K M, Hultman L, Gogotsi Y and Barsoum M W 2013 New two-dimensional niobium and vanadium carbides as promising materials for Li-ion batteries *J. Am. Chem. Soc.* **135** 15966–9
[24] Er D, Li J, Naguib M, Gogotsi Y and Shenoy V B 2014 Ti_3C_2 MXene as a high capacity electrode material for metal (Li, Na, K, Ca) ion batteries *ACS Appl. Mater. Interfaces* **6** 11173–9
[25] Naguib M, Mashtalir O, Carle J, Presser V, Lu J, Hultman L, Gogotsi Y and Barsoum M W 2012 Two-dimensional transition metal carbides *ACS Nano* **6** 1322–31
[26] Kresse G and Joubert D 1999 From ultrasoft pseudopotentials to the projector augmented-wave method *Phys. Rev.* B **59** 1758–75
[27] Grimme S, Antony J, Ehrlich S and Krieg H 2010 A consistent and accurate *ab initio* parametrization of density functional dispersion correction (DFT-D) for the 94 elements H-Pu *J. Chem. Phys.* **132** 154104
[28] Mills G, Jónsson H and Schenter G K 1995 Reversible work transition state theory: application to dissociative adsorption of hydrogen *Surf. Sci.* **324** 305–37
[29] Zhu J, Chroneos A, Eppinger J and Schwingenschlögl U 2016 S-functionalized MXenes as electrode materials for Li-ion batteries *Appl. Mater. Today* **5** 19–24
[30] Tang Q, Zhou Z and Shen P 2012 Are MXenes promising anode materials for li ion batteries? computational studies on electronic properties and li storage capability of Ti_3C_2 and $Ti_3C_2X_2$ (X = F, OH) monolayer *J. Am. Chem. Soc.* **134** 16909–16
[31] Tritsaris G A, Kaxiras E, Meng S and Wang E 2013 Adsorption and diffusion of lithium on layered silicon for Li-ion storage *Nano Lett.* **13** 2258–63
[32] Shu H, Li F, Hu C, Liang P, Cao D and Chen X 2016 The capacity fading mechanism and improvement of cycling stability in MoS_2-based anode materials for lithium-ion batteries *Nanoscale* **8** 2918–26
[33] Kumar R V and Sarakonsri T 2010 *Introduction to Electrochemical Cells* (Weinheim: Wiley) pp 1–25